Patronin mediates a switch from kinesin-13–dependent poleward flux to anaphase B spindle elongation

Haifeng Wang, Ingrid Brust-Mascher, Gul Civelekoglu-Scholey, and Jonathan M. Scholey

Department of Molecular and Cell Biology, University of California, Davis, Davis, CA 95616

Anaphase B spindle elongation contributes to chromosome segregation during *Drosophila melanogaster* embryo mitosis. We propose that this process is driven by a kinesin-5–generated interpolar microtubule (MT; ipMT) sliding filament mechanism that engages when poleward flux is turned off. In this paper, we present evidence that anaphase B is induced by the minus end–stabilizing protein Patronin, which antagonizes the kinesin-13 depolymerase KLP10A at spindle poles, thereby switching off the depolymerization of the minus ends of outwardly sliding ipMTs to suppress flux. Although intact cortices, kinetochore MTs, and midzone augmentation are dispensable, this Patronin-based change in ipMT minus-end dynamics is sufficient to induce the elongation of spindles capable of separating chromosomes.

Introduction

Chromosome segregation during mitosis involves chromosome to pole motility (anaphase A) and spindle elongation (anaphase B; Ris, 1943; Goshima and Scholey, 2010; Walczak et al., 2010; Drechsler and McAinsh, 2012; McIntosh et al., 2012). In *Drosophila melanogaster* embryos, whereas anaphase A depends on a combined pacman-flux mechanism (Rogers et al., 2004), we propose that anaphase B depends on a persistent kinesin-5–generated interpolar microtubule (MT; ipMT) sliding filament mechanism that "engages" to push apart the spindle poles when poleward flux is turned off (Cole et al., 1994; Kashina et al., 1996; Brust-Mascher and Scholey, 2002; Brust-Mascher et al., 2004, 2009; Cheerambathur et al., 2007; van den Wildenberg et al., 2008; de Lartigue et al., 2011; Acar et al., 2013). Thus, in preanaphase B spindles, the outward sliding of ipMTs is balanced by the depolymerization of their minus ends at the poles, producing poleward flux, and the spindle maintains a steady length (the "feeder–chipper mechanism"; Gadde and Heald, 2004). After cyclin B degradation, however, ipMT minus-end depolymerization ceases, so poleward flux is turned off, and the outwardly sliding ipMTs can now elongate the spindle. At the same time, ipMT plus ends display net growth and recruit MT–MT cross-linkers to assemble a more robust midzone where the sliding motors act.

Here, we tested our hypothesis that the specific stabilization of depolymerizing ipMT minus ends around the poles triggers anaphase B onset by investigating the roles of the kinesin-13 KLP10A (Rogers et al., 2004) and its antagonist, Patronin, which functions specifically to stabilize MT minus ends against kinesin-13–catalyzed depolymerization (Goodwin and Vale, 2010). The inhibition of Patronin and KLP10A produces short metaphase (Goshima et al., 2007) and collapsed or persistently elongating prometaphase spindles (Rogers et al., 2004), respectively, but their roles in anaphase B, when the biochemical and mechanical state of the spindle differs from these earlier mitotic phases, are unknown. We show that (a) Patronin counteracts KLP10A activity at spindle poles to turn off poleward flux and induce anaphase B spindle elongation, illustrating an important role for changes in ipMT minus-end dynamics; and (b) the inhibition of KLP10A activity is sufficient to initiate the elongation of nondegradable cyclin B–arrested spindles at a rate and extent characteristic of normal anaphase B.

Results and discussion

Patronin-GFP and KLP10A-GFP are dissociated from spindles by antibody microinjection

Fluorescence microscopy of live transgenic flies reveals that Patronin-GFP is positioned to protect MT minus ends throughout the spindle, whereas KLP10A could depolymerize MTs mainly

Correspondence to Jonathan M. Scholey: jmscholey@ucdavis.edu

Abbreviations used in this paper: ipMT, interpolar MT; kMT, kinetochore MT; MT, microtubule; NEB, nuclear envelope breakdown.

The Rockefeller University Press $30.00
J. Cell Biol. Vol. 203 No. 1 35–46
www.jcb.org/cgi/doi/10.1083/jcb.201306001

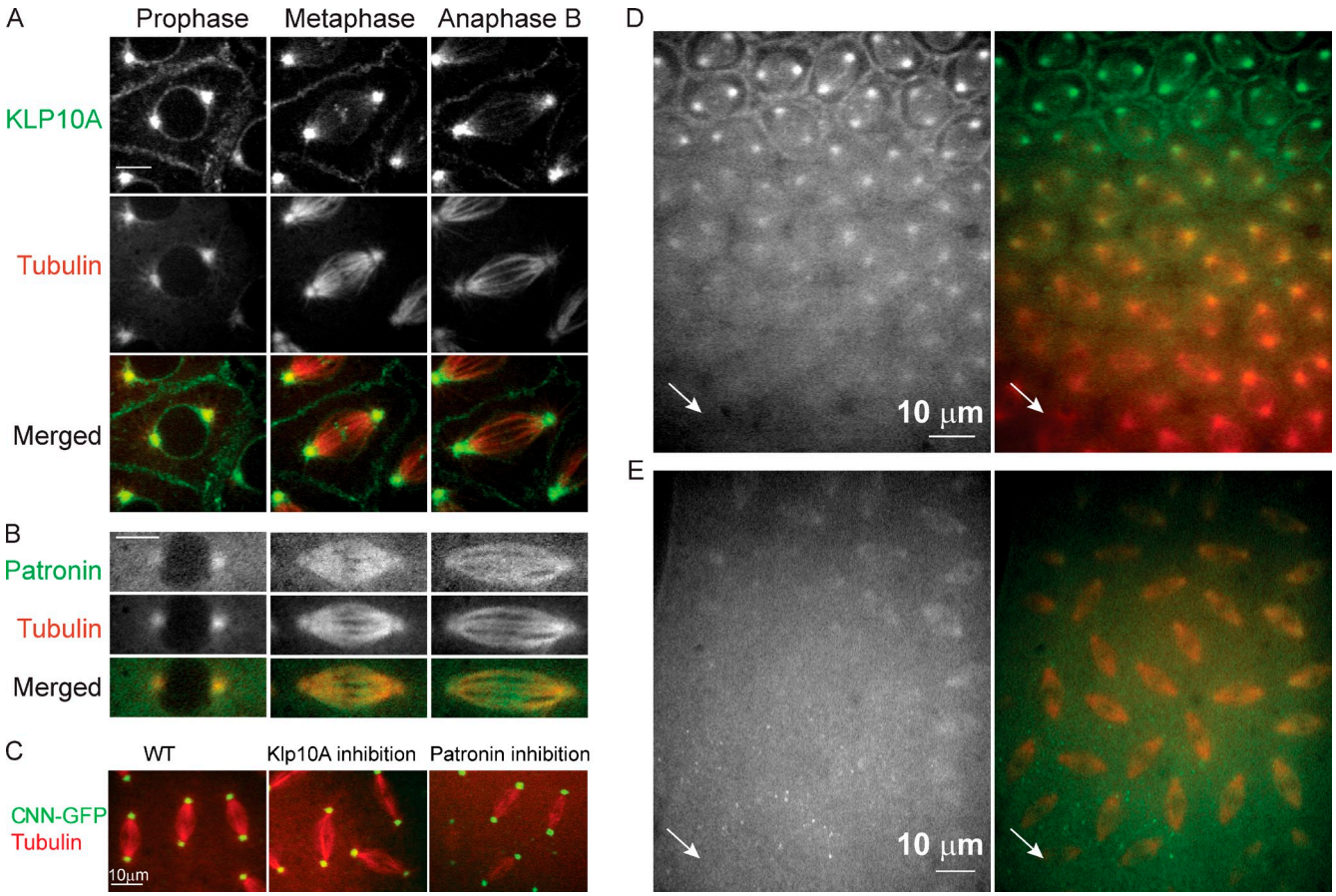

Figure 1. **Antibody-induced dissociation of KLP10A and Patronin from spindles.** (A and B) Live embryos expressing KLP10A-GFP (A) or Patronin-GFP (B, green in merged) injected with tubulin (red in merged). Bar, 5 µm. KLP10A-GFP (A and Video 1) localizes to spindle poles, kinetochores (from prometaphase to anaphase A) and faintly to cortices and spindle MTs. Patronin-GFP (B and Video 2) localizes to the mitotic spindle and interphase cytoplasm. (C) Anti-KLP10A or anti-Patronin antibody injections did not affect the integrity of spindle poles marked by centrosomin (CNN)-GFP. (D and E) Microinjection of anti-KLP10A (D) and anti-Patronin (E) dissociated their target antigens from spindles. Left images show KLP10A-GFP and Patronin-GFP alone, and right images show merged images of tubulin (red) and KLP10A-GFP or Patronin-GFP (green). Arrows show injection sites. WT, wild type.

around the poles, but it does not dissociate during anaphase B (Fig. 1, A and B; and Videos 1 and 2; Rogers et al., 2004; Goshima and Vale, 2005; Goodwin and Vale, 2010). As in a study of kinesin-5 (Brust-Mascher et al., 2009), microinjected anti-KLP10A and anti-Patronin rapidly displaced their target antigen from spindles, forming fluorescent cytoplasmic immunoprecipitates (Fig. 1, D and E). In spindles depleted of KLP10A, we observed premature prometaphase spindle elongation (see Fig. 3 D), as expected (Rogers et al., 2004). In antibody-injected centrosomin-GFP–expressing embryos, spindle poles remain intact, so these antibodies do not influence MT dynamics by disorganizing spindle poles (Fig. 1 C).

Patronin inhibition suppresses anaphase B spindle elongation

To examine whether the Patronin-mediated stabilization of ipMT minus ends induces anaphase B, we inhibited Patronin by injecting anti-Patronin into embryos expressing GFP-tubulin and RFP-histone. The injected antibody diffuses throughout the syncytium to form a concentration gradient, thereby producing a range of phenotypes equivalent to an allelic series of mutants whose severity decreases with decreasing antibody concentration moving away from the injection site (Fig. 2 A and Fig. S1 B). Accordingly, spindles closest to the injection site displayed delayed, incomplete chromosome segregation and no anaphase B spindle elongation, whereas distal spindles displayed normal chromosome segregation and anaphase B (Fig. 2 A).

We quantified the phenotype of four to five spindles in several embryos close to the injection site (Fig. S1 C). Interestingly, although previous studies revealed that Patronin RNAi significantly decreased *Drosophila* S2 cell metaphase spindle length, the anti-Patronin antibody produced very few short (4%) or abnormal (3%) embryonic metaphase spindles with the majority (92%) being of normal length (Fig. 2 E; Goshima et al., 2007; Goodwin and Vale, 2010). However, anaphase B was not evident in 69% of spindles, and within 92% of these, chromosomes remained linked at the equator, and only their leading edges reached the poles (Fig. S1 C).

To better characterize these spindle phenotypes, we acquired z stacks extending through 4 µm. In controls (Fig. 2 B, top; and Video 3), anaphase B spindle elongation was observed 30–40 s after anaphase A onset. Patronin inhibition suppressed anaphase B but anaphase A proceeded at normal rates after a delay (Fig. 2, B [bottom], C, and E; and Video 4). Chromosome segregation was often incomplete (Fig. 2, A and B; and Fig. S1 B),

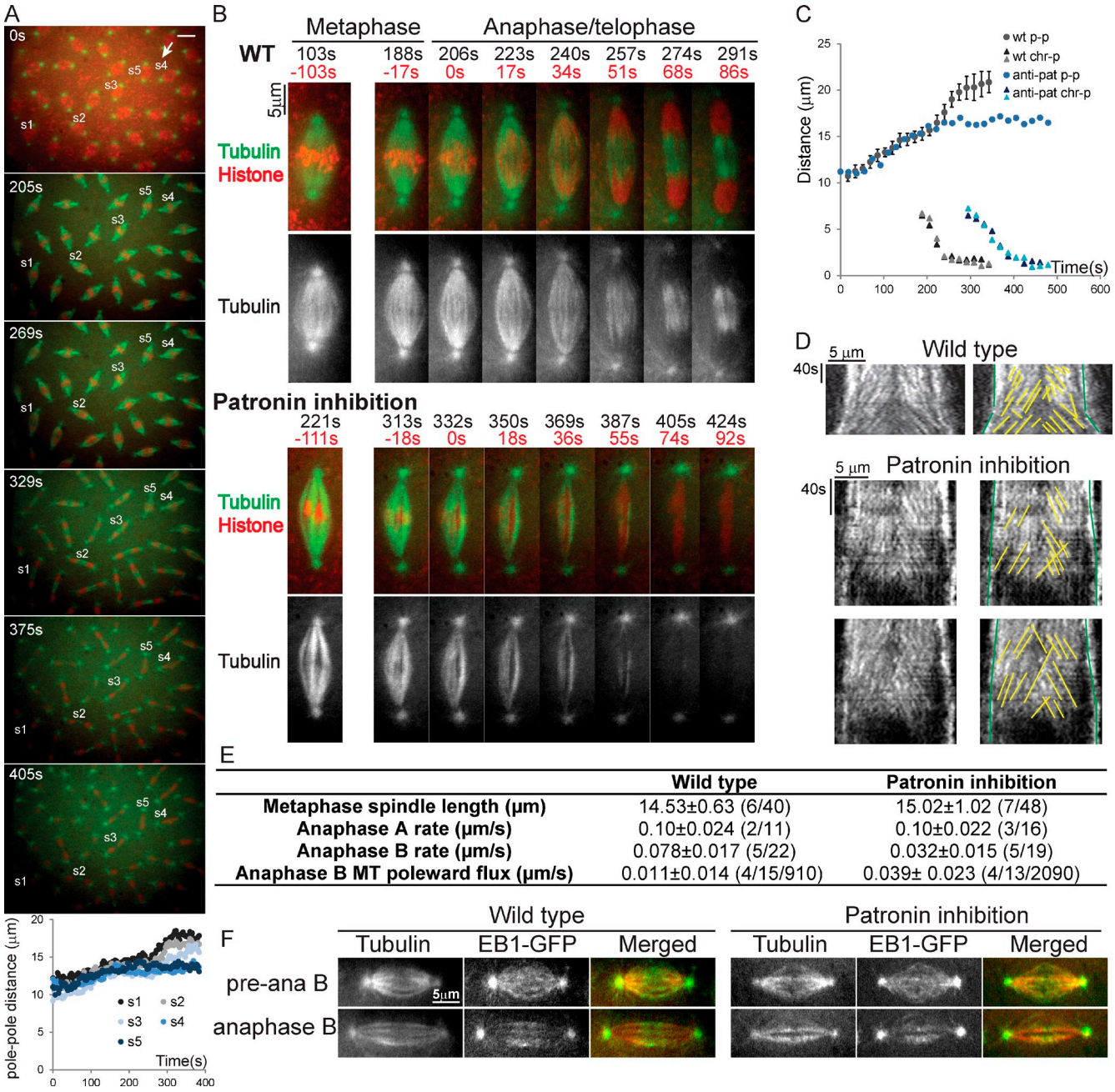

	Wild type	Patronin inhibition
Metaphase spindle length (μm)	14.53±0.63 (6/40)	15.02±1.02 (7/48)
Anaphase A rate (μm/s)	0.10±0.024 (2/11)	0.10±0.022 (3/16)
Anaphase B rate (μm/s)	0.078±0.017 (5/22)	0.032±0.015 (5/19)
Anaphase B MT poleward flux (μm/s)	0.011±0.014 (4/15/910)	0.039± 0.023 (4/13/2090)

Figure 2. **Patronin stabilizes MT minus ends and is necessary for anaphase B spindle elongation.** (A) Time-lapse images and spindle length plots of a representative embryo injected with anti-Patronin (arrow) at NEB (0 s) showing a gradient of phenotypes. Green, tubulin. Red, histone. Spindles close to the injection site (spindle 4 [s4] and spindle 5 [s5]) display normal metaphase length but no anaphase B spindle elongation, whereas distal spindles (spindle 1 [s1] and spindle 2 [s2]) show normal anaphase B. Repeated in >25 embryos. Bar, 10 μm. (B) Representative spindle after Patronin inhibition (bottom) compared with control (top). Black, time from NEB; red, time from anaphase A onset. See also Videos 3 and 4. (C) Plots of pole–pole (p-p) and chromosome to pole (chr-p) distances versus time for control and anti-Patronin (pat)–injected embryos. NEB = 0 s. Error bars show SDs. (D) Representative tubulin kymographs after Patronin inhibition (bottom) compared with control (top). (right) Yellow and green lines track tubulin speckles and spindle poles, respectively. Sharpen and low-pass filters were applied. (E) Quantitation (±SDs). Patronin inhibition decreased the anaphase B spindle elongation rate ($P = 1.553 \times 10^{-10}$) and increased the rate of anaphase B MT poleward flux ($P < 2.2 \times 10^{-16}$), without decreasing preanaphase B spindle length or the anaphase A chromosome to pole rate. For anaphase B measurements, we have included spindles in the gradient with suppressed anaphase B, which allowed us to distinguish anaphase B from preanaphase B. The number of embryos (first number), spindles (second number), and speckles (third number) analyzed are indicated in parentheses. (F) EB1-GFP localization in wild-type and Patronin-inhibited embryos during preanaphase (pre-ana) B and anaphase B. Red, tubulin; green, EB1. WT, wild type.

but whether this is a secondary effect of anaphase B perturbation or a direct effect on kinetochore MTs (kMTs) requires further work. After anaphase A, spindle MTs rapidly disappeared, and no telophase midzone assembled. The results support the hypothesis that Patronin may normally induce anaphase B by protecting MT minus ends against KLP10A activity so that its inhibition exposes MT minus ends to KLP10A-mediated depolymerization.

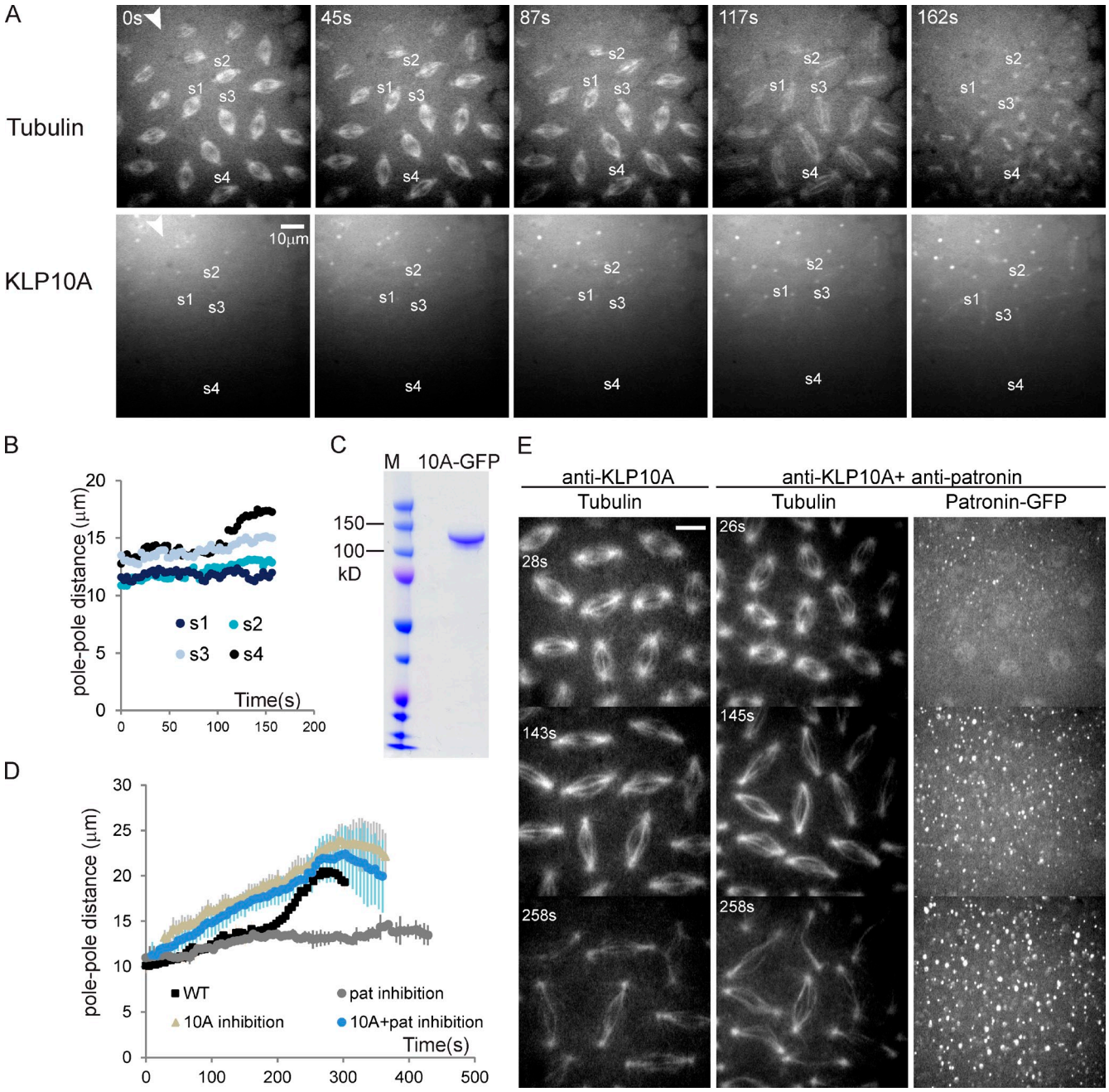

Figure 3. **Functional antagonism between Patronin and KLP10A.** (A–C) Excess KLP10A-GFP inhibited anaphase B spindle elongation. Stills (A) and pole–pole distance versus time (B) for a representative embryo microinjected with purified KLP10A-GFP, which formed a visible concentration gradient and localized normally (A, bottom). Close to the injection site (arrowheads, *t* = 0 s), KLP10A depolymerase activity destabilized metaphase spindles, whereas more distal metaphase spindles were stable but displayed no anaphase B spindle elongation (spindles 1 and 2 [s1 and s2]). Mitosis was normal at very distal sites (e.g., spindle 4 [s4]). Repeated in >20 embryos. (C) SDS-PAGE of microinjected KLP10A-GFP. M, protein markers. (D and E) Co-depletion of Patronin (pat) and KLP10A caused persistent spindle elongation from prometaphase on, just like KLP10A inhibition alone. (D) Pole–pole distance versus time from NEB (0 s) in injected embryos. Error bars show SDs. (E) Time-lapse images of embryos injected with anti-KLP10A (left) or with both anti-Patronin and anti-KLP10A (middle and right). Right images show that Patronin dissociated from spindles to form cytoplasmic immunoprecipitates. 0 s = NEB. Bar, 10 μm.

Patronin inhibition deprotects MT minus ends, allowing poleward flux to persist during anaphase B

The rate of poleward MT flux, i.e., the rate of tubulin speckle velocity minus the rate of pole motility, reflects the extent of MT depolymerization at the poles. Patronin inhibition during anaphase B led to an increase in the poleward flux rate with a corresponding decrease in the spindle elongation rate (Fig. 2, D and E), although EB1-GFP–bound MT plus ends concentrated normally at the equator (Fig. 2 F; Cheerambathur et al., 2007). This is consistent with the hypothesis that Patronin specifically protects MT minus—but not plus—ends (Goodwin and Vale, 2010) and could induce anaphase B by specifically protecting minus ends around the poles from KLP10A activity.

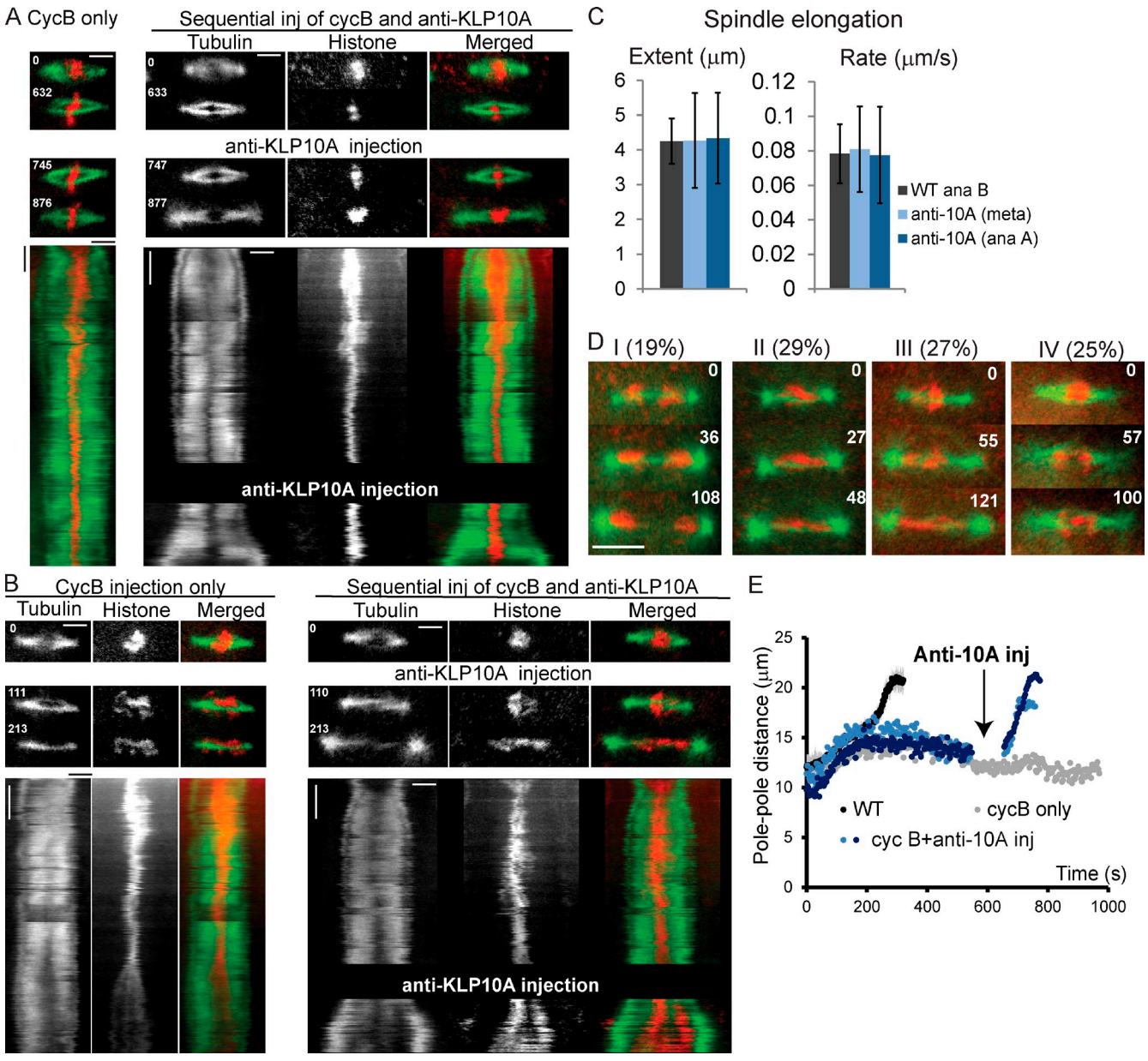

Figure 4. **KLP10A inhibition is sufficient to induce anaphase B spindle elongation in preanaphase B–arrested spindles.** (A and B) KLP10A inhibition in spindles arrested at metaphase (A; Video 5) or anaphase A (B; Videos 6 and 7). (left) Control spindles injected only with cyclin B (see also Fig. S1, E and F). (right) Spindles sequentially injected (inj) with cyclin B (CycB) and anti-KLP10A (see also Fig. S2 A). Top two rows show representative micrographs, and the bottom row shows corresponding kymographs. Time is in seconds from prometaphase (A) or anaphase A onset (B). Green, tubulin; red, histone. Bars: (horizontal) 5 μm; (vertical) 100 s. (C) In embryos sequentially injected with cyclin B and anti-KLP10A, the extent ($P = 0.8609$) and rate ($P = 0.7766$) of elongation of spindles arrested in metaphase (meta; 21 spindles in 9 embryos) or anaphase A (ana; 21 spindles in 7 embryos) were indistinguishable from wild-type anaphase B (22 spindles in 5 embryos). Error bars show SDs. (D) Anaphase A–arrested spindles (52 spindles in 11 embryos) were classified as (I) spindle elongation followed anaphase A and led to complete chromosome segregation (19%); (II) spindle elongation occurred after anaphase A, but lagging chromosomes or chromosome bridges formed (29%); (III) spindle elongation accompanied anaphase A, and bridges were present on chromosomes whose leading edges reached the poles (27%); and (IV) spindle elongation occurred with incomplete anaphase A, and the leading edges of chromosomes did not reach the poles (25%). Bar, 10 μm. 0 s = anti-KLP10A injection time. See also Fig. S2 B. (E) Spindle pole dynamics from NEB (0 s) in (a) an untreated embryo (wild type [WT]), (b) a representative embryo injected only with cyclin B before NEB (cyclin B [cycB] only), and (c) a representative embryo injected with cyclin B before NEB and anti-KLP10A at the indicated time (cyclin B + anti-KLP10A [anti-10A]). Repeated in >25 embryos. See also Fig. S2 A.

Patronin and KLP10A function antagonistically to regulate anaphase B spindle elongation

In a concentration gradient of microinjected excess KLP10A-GFP, zones of high, low, and intermediate concentrations displayed (a) metaphase spindle disassembly, (b) normal mitosis, and (c) short metaphase spindles with no anaphase B, respectively (Fig. 3, A–C). Thus, adding kinesin-13 to spindles, like depletion of Patronin, can inhibit anaphase B. Moreover, coinjected anti-KLP10A and anti-Patronin (which efficiently displaced Patronin from spindles; Fig. 3 E, right) caused persistent elongation of prometaphase spindles, just like anti-KLP10A

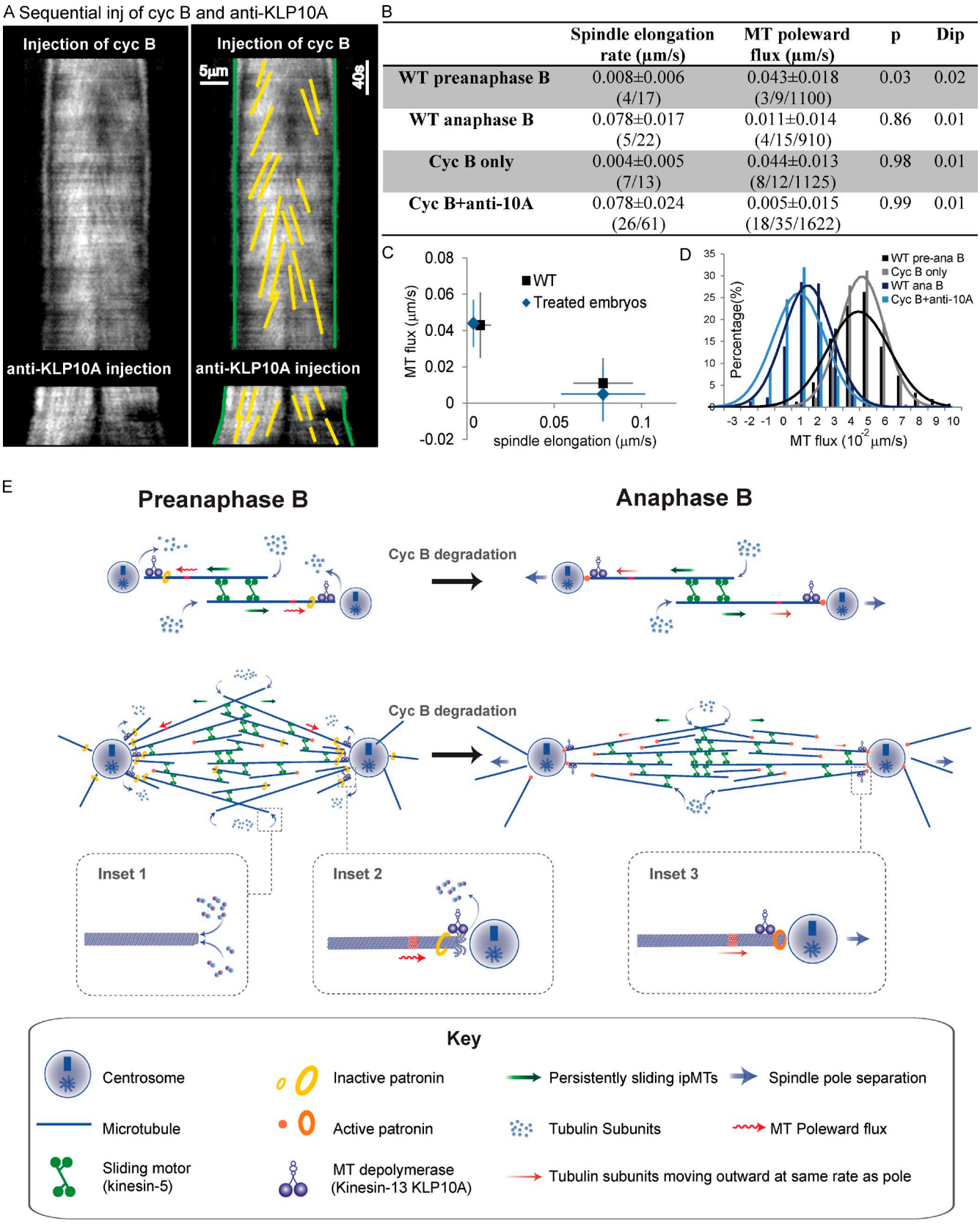

	Spindle elongation rate (µm/s)	MT poleward flux (µm/s)	p	Dip
WT preanaphase B	0.008±0.006 (4/17)	0.043±0.018 (3/9/1100)	0.03	0.02
WT anaphase B	0.078±0.017 (5/22)	0.011±0.014 (4/15/910)	0.86	0.01
Cyc B only	0.004±0.005 (7/13)	0.044±0.013 (8/12/1125)	0.98	0.01
Cyc B+anti-10A	0.078±0.024 (26/61)	0.005±0.015 (18/35/1622)	0.99	0.01

Figure 5. **KLP10A inhibition converts MT poleward flux to spindle elongation, mimicking the anaphase B switch.** (A) Representative tubulin kymograph from an embryo sequentially injected with cyclin B and anti-KLP10A to monitor poleward flux. Yellow and green lines track tubulin speckles and spindle poles, respectively. Sharpen and low-pass filters were applied. (B) Comparison of spindle elongation and poleward flux rates in wild-type and injected embryos (±SDs; cyc B only, injected with only cyclin B; cyc B+anti-10A, sequentially injected with cyclin B and anti-KLP10A). KLP10A inhibition significantly decreased MT poleward flux rate ($P < 2.2 \times 10^{-16}$), as observed at anaphase B onset in wild-type embryos ($P < 2.2 \times 10^{-16}$). P-values and dip values from

alone (Fig. 3, D and E). These observations suggest that Patronin works upstream of KLP10A, with Patronin protecting and KLP10A depolymerizing the minus ends of MTs, respectively.

Inhibition of KLP10A induces anaphase B–like spindle elongation in preanaphase B–arrested spindles

To investigate whether turning off KLP10A depolymerase activity is sufficient to induce the elongation of spindles maintained at their steady-state preanaphase B length, we experimentally inhibited KLP10A in metaphase- or anaphase A–arrested spindles (Fig. 4, Fig. S2, and Videos 5, 6, and 7; Cheerambathur et al., 2007). In cycle 11 controls, spindles maintain a constant length of 14–16 µm for 1–2 min during preanaphase B before elongating to ≥20 µm during anaphase B, starting ∼40 s after anaphase A onset. Microinjection of nondegradable cyclin B arrested spindles at a constant length in metaphase (intracellular cyclin B concentration: ∼0.7 mg/ml; Fig. 4 A, left; and Fig. S1 E) or after anaphase A onset (∼0.3 mg/ml cyclin B; Fig. 4 B, left; and Fig. S1 F). The subsequent microinjection of anti-KLP10A induced spindle elongation at a similar rate and extent as wild-type anaphase B (Fig. 4, A–C; Fig. S2 A; and Videos 5, 6, and 7). In metaphase-arrested spindles, chromosomes remained at the spindle equator (Fig. 4 A, right; and Video 5), but in anaphase A–arrested spindles, pole–pole separation induced by KLP10A inhibition further separated the leading edges of chromosomes (Fig. 4 B, right; Fig. S2 A; and Videos 6 and 7). This suggests that turning off the KLP10A depolymerase activity at spindle poles is sufficient to tip the balance of forces that maintains the preanaphase B spindle at its steady-state length and can induce anaphase B spindle elongation both with intact kMTs and after kMTs have depolymerized.

Anaphase B–like spindle elongation induced by KLP10A inhibition can move chromosomes apart

In these cyclin B and anti-KLP10A double-injection experiments, anaphase A–arrested spindles fall into four classes (Fig. 4 D and Fig. S2 B). In class I and II, the leading edges of both sets of chromosomes reached the poles before spindle elongation and then separated at a rate similar to the rate of pole–pole separation, whereas chromosome to pole spacing remained unchanged, suggesting that the spindle elongation induced by KLP10A inhibition contributed to the segregation of chromosomes. In class III, one or both leading edges moved toward its proximal pole during spindle elongation consistent with anaphase A and B acting together. In class IV, anaphase A initiated but then stalled so that chromatin masses remained near the equator throughout anaphase B. Thus, in class I–III, spindle elongation contributed to chromosome separation as in wild-type anaphase B, although only class I had fully segregated chromosomes.

Anaphase B–like spindle elongation induced by KLP10A inhibition is independent of cortical forces and robust midzone assembly

In syncytial embryos, cortical pulling forces (Sharp et al., 2000; Saunders et al., 2007; Telley et al., 2012) appear to play little role in anaphase B spindle elongation. Accordingly, when we inhibited KLP10A (a minor fraction of which localizes to cortices; Fig. 1 A) in cyclin B–arrested *scrambled* mutants containing severely disrupted cortices (Stevenson et al., 2001), we observed spindle elongation at a similar rate (0.078 ± 0.017 µm/s) to that observed in wild-type embryos (0.078 ± 0.024 µm/s; Fig. S2 C). The redistribution of ipMT plus ends to the equator at anaphase B onset, which is postulated to augment the midzone (Cheerambathur et al., 2007), is dispensable as well because when KLP10A was inhibited in cyclin B–arrested spindles, the ipMT plus ends marked by EB1-GFP did not concentrate in the midzone during spindle elongation (Fig. S2 D). In addition, we did not observe the midzone accumulation of the MT cross-linker, Feo (fascetto), normally seen in wild types (Fig. S2 E; Vernì et al., 2004). We note that inhibiting either Patronin (Fig. 2 F) or KLP10A (Fig. S2 D) uncoupled MT plus-end redistribution from spindle elongation, suggesting that these events may occur independent of one another at anaphase B onset.

KLP10A inhibition couples the suppression of poleward flux within ipMTs to spindle elongation, mimicking the wild-type anaphase B switch

Our model predicts that KLP10A inhibition in cyclin B–arrested spindles should suppress poleward flux to turn on anaphase B–like spindle elongation. After cyclin B injection, all spindles arrested in preanaphase B displayed persistent MT poleward flux at rates similar to wild types. The subsequent injection of anti-KLP10A suppressed poleward flux similar to the suppression of poleward flux at wild-type anaphase B onset (Fig. 5, A–D) and an inverse correlation between rates of flux and spindle elongation was observed (Fig. 5 C). Therefore, the inhibition of KLP10A alone can suppress poleward MT flux to induce anaphase B spindle elongation (Brust-Mascher et al., 2004).

Hartigan's dip test reveal unimodal flux data, except for wild-type (WT) preanaphase B spindles, in which it is bimodal ($P < 0.05$). The number of embryos (first number), spindles (second number), and speckles (third number) analyzed are indicated in parentheses. (C) MT poleward flux and spindle elongation rates in B are inversely correlated in both wild-type anaphase B switch and treated embryos. Error bars show SDs. (D) Histograms of the MT poleward flux rates shown in B (counts in B). The curves show the best-fit normal distributions. ana, anaphase. (E) Model of anaphase B induction in *Drosophila* syncytial embryos in which kinesin-5 persistently slides apart antiparallel ipMTs, and anaphase B spindle elongation is induced by a Patronin-mediated spindle pole–associated switch. During preanaphase B, KLP10A depolymerizes the minus ends of outward sliding ipMTs at the spindle poles, producing poleward flux in spindles maintained at a constant length. Cyclin B degradation induces an unknown Patronin modification that enhances its activity to protect ipMT minus ends from KLP10A-induced depolymerization at the poles, thus allowing outwardly sliding ipMTs to exert force and push apart the spindle poles. (top) Simplified model showing a single ipMT bundle, with minus ends reaching the poles. (bottom) More realistic model in which Patronin-bound ipMT minus ends localize all over the spindle, kinesin-5 slides antiparallel MTs apart, and KLP10A concentrates at spindle poles.

Patronin and KLP10A are thought to act on kMTs as well as ipMTs, so to ensure that our experiments report effects within ipMTs, we optimized the cyclin B injection dose to specifically select anaphase A–arrested spindles in which kMTs have significantly depolymerized, and this was corroborated by statistical analysis of the flux data. A Hartigan's dip test (Fig. 5 B; Hartigan, 1985; Hartigan and Hartigan, 1985) reveals bimodality in the wild-type preanaphase B flux data because of the presence of two distinct populations of speckles moving at slightly different rates, presumably corresponding to poleward flux in ipMTs and kMTs ($P < 0.05$). In contrast, the corresponding data from wild-type anaphase B and cyclin B– and cyclin B plus anti-KLP10A–injected embryos were all unimodal ($P > 0.8$) consistent with the flux data being derived only from ipMTs (Fig. 5 B). Thus, our results report the effect of KLP10A inhibition on the coupling between poleward flux and antiparallel MT sliding specifically within ipMTs.

Modeling predicts that a ninefold increase in the ratio of Patronin to KLP10A activity at spindle poles induces anaphase B

Analysis of KLP10A-GFP (Fig. 1 A and not depicted) and Patronin-GFP (Fig. 1 B and Fig. S3, A and B) suggests that changes in the activity of Patronin relative to KLP10A at spindle poles can induce anaphase B with no change in the localization or dynamics of either protein. To test this, we developed a computational model representing a half-spindle consisting of a fixed number of MTs sliding poleward, whose minus ends are depolymerized at the poles at a rate determined by the ratio of Patronin to KLP10A activity (Materials and methods; Table S1 and Fig. S3 C). In silico FRAP was used to determine KLP10A and Patronin on and off rates that gave similar half-times and recoveries to those observed in vivo (Fig. S3, B and G). We found that (a) assuming equal total concentrations of Patronin and KLP10A, depolymerization of multiple MT minus ends at a rate determined by stochastically binding and dissociating active Patronin and KLP10A yielded a stable front of MT minus ends; and (b) a ninefold increase in Patronin to KLP10A activity at anaphase B onset could reproduce the observed rate of spindle elongation (Fig. S3).

This increase in Patronin activity can plausibly induce anaphase B spindle elongation by protecting MT minus ends against KLP10A-induced depolymerization, independent of the redistribution of ipMT plus ends to the spindle equator. Thus, the anaphase B switch in *Drosophila* embryos involves (a) Patronin-mediated suppression of KLP10A activity, which is sufficient to convert MT poleward flux to anaphase B spindle elongation; and (b) spindle midzone reorganization, including redistribution of MT plus ends and accumulation of cross-linkers, which is dispensable for anaphase B, and whose function is unknown (Fig. 5 E).

Spindle length regulation by changes in MT minus- and plus-end dynamics

In our model, anaphase B induction depends on changes in the dynamics of the minus ends of ipMTs that reach the poles by sliding, but could changes in plus-end dynamics be involved? In the "slide-and-cluster" model, for example, the steady-state length of *Xenopus laevis* metaphase spindles depends on the rate of poleward transport (flux) of MTs nucleated at the chromosomes, together with their lifetime ($t_{1/2}$) during transport, which in turn is determined solely by the dynamics of their plus ends (Burbank et al., 2007; Brugués et al., 2012). In this scenario, it seems theoretically possible that the modulation of MT lifetime ($t_{1/2}$) solely via controlled changes in MT plus-end dynamics could produce spindle length changes throughout mitosis, including anaphase B. Kinesin-13 depolymerizes MTs from both ends (Desai et al., 1999), but the spindle elongation induced by KLP10A inhibition is unlikely to be caused by effects on MT plus-end dynamics because (a) Patronin is a specific MT minus-end protector (Goodwin and Vale, 2010), so it is unlikely to control MT plus-end dynamics at anaphase B onset; and (b) kinesin-8 specifically depolymerizes MT plus ends (Varga et al., 2006), and its inhibition in *Drosophila* produces premature spindle elongation accompanied by an increase, not a decrease, in poleward flux (Wang et al., 2010). Moreover, it is notable that other models of *Xenopus* spindle length control are clearly based on the control of MT minus-end dynamics at spindle poles in agreement with our model for anaphase B in *Drosophila* embryos (Loughlin et al., 2010, 2011).

It remains to be seen how conserved is this proposed mechanism for spindle elongation because of the likely existence of system-specific variations. For example, in *Drosophila* embryos and S2 cells, the mechanism of anaphase B is qualitatively, but not quantitatively, conserved, with poleward flux often being only partially suppressed to initiate elongation of S2 cell spindles (Brust-Mascher et al., 2009; de Lartigue et al., 2011); in fission yeast, poleward flux and MT depolymerization at spindle poles cannot be detected (Mallavarapu et al., 1999); in *Caenorhabditis elegans* embryos, cortical forces elongate the spindle (Saunders et al., 2007); and mouse meiosis is topsy-turvy, with anaphase B occurring before anaphase A, unlike in most systems (FitzHarris, 2012). Therefore, although it is likely that spindle length control via changes in MT minus-end dynamics may be broadly conserved (Rogers et al., 2004; Dumont and Mitchison, 2009; Loughlin et al., 2010, 2011), a variety of mechanisms may exist for controlling spindle length in different cell types during different stages of mitosis including anaphase B (Goshima and Scholey, 2010).

Our evidence suggests that, in *Drosophila* embryos, after cyclin B degradation, the up-regulation of Patronin activity, by an as yet to be determined mechanism, antagonizes KLP10A leading to ipMT minus-end stabilization and the initiation of anaphase B spindle elongation. Our data reveal that a Patronin-based switch in ipMT minus-end dynamics could account for the rate and extent of anaphase B spindle elongation.

Materials and methods

Generation of transgenic flies

A full-length KLP10A cDNA tagged with GFP was subcloned from a pMT vector, provided by G. Goshima (Nagoya University, Nagoya, Japan) and R. Vale (University of California, San Francisco, San Francisco, CA; Goshima and Vale, 2005), into the pWR-pUbq vector (provided by N. Brown, University of Cambridge, Cambridge, England, UK) downstream of the polyubiquitin promoter. A full-length Patronin cDNA clone was

ordered from the Drosophila Genomics Resource Center (AT18914), corrected to encode Patronin isoform A (NCBI database accession no. NP_788398), tagged with a GFP coding sequence after removing the stop codon, and then subcloned into the pWR-pUbq vector. A full-length Feo cDNA was obtained by RT-PCR (encoding NP_572658; NCBI), and then subcloned with a GFP coding sequence into the pWR-pUbq vector in a similar way. Transgenic flies with a single insertion in the second chromosome were generated with each construct by BestGene, Inc.

Drosophila stocks and embryo preparation

All flies were maintained at 25°C according to standard procedures, and embryos were collected on grape juice plates, dechorionated, and kept in halocarbon oil during imaging and microinjections (Brust-Mascher et al., 2009). Transgenic flies coexpressing GFP-tubulin and RFP-histone were generated by crossing flies expressing GFP-tubulin (provided by T. Kaufman, Indiana University, Bloomington, IN) with flies expressing histone-RFP (obtained from Bloomington Drosophila Stock Center; Civelekoglu-Scholey et al., 2010; Wang et al., 2010). Flies expressing GFP-histone were provided by P. O'Farrell (University of California, San Francisco, San Francisco, CA; Parry and O'Farrell, 2001). Flies with an EB1-GFP transgene were provided by S. Rogers (University of North Carolina at Chapel Hill, Chapel Hill, NC), B. Eaton, and G. Davis (University of California, San Francisco, San Francisco, CA) and expressed by standard crossing (Rogers et al., 2002; Wang et al., 2010). Flies expressing GFP-cid were provided by S. Henikoff (Fred Hutchinson Cancer Research Center, Seattle, WA; Henikoff et al., 2000). Flies expressing GFP-centrosomin were provided by T. Kaufman (Indiana University, Bloomington, IN).

Protein purification, antibody generation, and microinjection

The anti-KLP10A antibody was affinity purified with Maltose-binding protein–tagged KLP10A N-terminal fragment (1–213 aa) from a rabbit anti-KLP10A serum against GST-tagged KLP10A N terminus (Rogers et al., 2004). GST–cyclin B was expressed in *Escherichia coli* and purified with glutathione agarose (Thermo Fisher Scientific; Kellogg et al., 1995; Cheerambathur et al., 2007). The anti-Patronin antibody was affinity purified with GST-tagged Patronin C-terminal fragment (1,313–1,517 aa of NP_788398 in NCBI) from rabbit anti-Patronin serum against His-tagged Patronin C-terminal fragment (Goodwin and Vale, 2010), provided by M. Hendershott, S. Goodwin, and R. Vale (University of California, San Francisco, San Francisco, CA). To purify wild-type KLP10A-GFP protein, KLP10A-GFP cDNA tagged with C-terminal 6×His tag was cloned to pDEST 8 vector (Invitrogen) and expressed in the SF9 cell baculovirus system. The SF9 cell pellet was collected, lysed by French press, and centrifuged at 35,000 rpm for 37 min on a rotor (Ti 50.2; Beckman Coulter), and the supernatant was incubated with Ni–nitrilotriacetic acid agarose (QIAGEN), washed, and then eluted in a Tris-based buffer, pH 8.0, containing 300 mM Imidazole (Tao et al., 2006). All injected proteins were dialyzed in PBS and concentrated before injection. The injected protein concentrations were determined by Bradford assays: anti-Patronin antibody at 50 mg/ml, cyclin B at 50 mg/ml, anti-KLP10A antibody at 80 mg/ml, and KLP10A-GFP at 20 mg/ml.

Most embryos were injected in cycle 10 or 11 and were immediately imaged after microinjection (30–120 s). All shown spindles, except those within a gradient, were within 50 µm distance of the injection site, and the injection site was determined by approximate eye observation and confirmed by the most severe phenotypes. In figures showing a gradient of effects (Fig. 1, D and E; Fig. 2 A; Fig. 3 A; and Fig. S1 B), the injection sites are shown in the first frame. The mean intracellular concentrations were calculated as protein concentration × estimated injection volume/embryo volume and were at ∼0.3 mg/ml for the anti-Patronin antibody, ∼0.3 mg/ml for low dose cyclin B, ∼0.7 mg/ml for high dose cyclin B, ∼0.5 mg/ml for the anti-KLP10A antibody, and ∼0.1 mg/ml for KLP10A-GFP. For Patronin inhibition experiments, embryos were injected with Patronin antibody (intracellular concentration: ∼0.3 mg/ml) around nuclear envelope breakdown (NEB) and imaged during the following cycle. For KLP10A inhibition experiments, embryos were injected with ∼0.5 mg/ml anti-KLP10A antibody around NEB and imaged during the following cycle. For the co-depletion of Patronin and KLP10A experiment, embryos were injected with ∼0.3 mg/ml anti-Patronin and ∼0.5 mg/ml anti-KLP10A around NEB and imaged during the following cycle. For the KLP10A-GFP injection experiment, embryos were injected with purified ∼0.1 mg/ml KLP10A-GFP before metaphase and imaged right after injection. For each cyclin B and anti-KLP10A sequential injection experiment, cyclin B was injected around NEB onset, the injected embryo was imaged under the microscope to ensure spindles arrested in preanaphase B, and then, ∼0.5 mg/ml anti-KLP10A was injected close to the cyclin B injection site, and the embryo was returned to the confocal microscope for continued imaging. For example, in Fig. 4 A, cyclin B injection (performed at >80 s [Fig. 4 A, left] or >3 s [Fig. 4 A, right]) before prometaphase (0 s) arrested the spindles in metaphase, and then, anti-KLP10A injection was performed between 633 and 747 s (Fig. 4 A, right). In Fig. 4 B, after cyclin B injection, the spindles were recorded for 634 s (Fig. 4 B, left) or 545 s (Fig. 4 B, right) before anaphase A onset (0 s) to make sure that they arrested in preanaphase B, and anti-KLP10A was injected between 0 and 110 s (Fig. 4 B, right). Embryos were premicroinjected with rhodamine-tubulin (Cytoskeleton, Inc.) for all fluorescence speckle microscopy experiments and when necessary to visualize tubulin.

Microscope image acquisition and data analysis

Time-lapse images (of GFP/RFP-labeled proteins or rhodamine-tubulin) were acquired on an inverted microscope (IX70; Olympus) equipped with a spinning-disk confocal head (UltraVIEW; PerkinElmer), a 100×, 1.35 NA or 60×, 1.4 NA oil immersion objective, and a charge-coupled device camera (ORCA ER; Hamamatsu Photonics) using Volocity software (PerkinElmer). Either a single confocal plane or a stack of nine planes spaced by 0.5 µm was acquired at time intervals of 0.5–20 s at room temperature (20–22°C).

FRAP experiments (with GFP-labeled proteins) were performed on a laser-scanning confocal microscope (FV1000; Olympus) with a 60×, 1.40 NA oil immersion objective at 23°C, and images were acquired using the FluoView software (version 1.5; Olympus). A 405-nm laser at 40% power was used to photobleach small circular regions in different areas of the spindle during preanaphase and anaphase B. Images were acquired with a 488-nm laser at rates of four to 5 frames/s. All data were corrected for photobleaching and normalized by $I(t) = [F(t)\ T_{pre}]/[T(t)\ F_{pre}]$, in which $F(t)$ and $T(t)$ are the mean fluorescence in the FRAP region and in the entire spindle at time t, and F_{pre} and T_{pre} are the mean fluorescence in the FRAP region and in the entire spindle just before the bleach (Phair and Misteli, 2000; Lele et al., 2006). The recovery curve was fitted with an exponential equation $F_{fit}(t) = F_0 + (F_{inf} - F_0)(1 - e^{-kt})$, in which k is a constant describing the rate of recovery, F_0 is the fluorescence immediately after the bleach, and F_{inf} is the maximum recovered fluorescence. The recovery half-time was calculated by $t_{1/2} = \ln 2/k$, and the percentage of fluorescence recovery was given by $(F_{inf} - F_0)/(F_{pre} - F_0)$.

Images were analyzed with MetaMorph Imaging software (Universal Imaging). Pole and chromosome leading edge positions were logged in each image. For Fig. 2 E, metaphase spindle length was quantified during cycle 10. Pole to pole and chromosome to pole distances as functions of time were calculated from these positions. Anaphase A chromosome to pole and anaphase B spindle elongation rates were measured as the maximum rates. For tubulin fluorescent speckle microscopy, sharpen and low-pass filters were applied to all images, and tubulin speckle/pole movement was quantified from kymographs. MT poleward flux rates were calculated by subtracting pole movement from raw tubulin speckle velocities.

Calculations and statistical analyses were performed on Excel (Microsoft). All value comparisons were performed using the Wilcoxon rank sum test on R (R Project). The Hartigan's dip test (performed using MATLAB) is used to determine unimodality in a sample distribution by the maximum difference, over all sample points, between the empirical distribution function, and the unimodal distribution function that minimizes that maximum difference (Hartigan, 1985; Hartigan and Hartigan, 1985). All error bars shown in the figures are SDs.

Modeling methods: Model description and assumptions

The model consists of a parallel array of MTs (typically 3–15) representing the MTs in a half-spindle ipMT bundle (Fig. S3 C), organized with their plus ends toward the equator, and a fixed total number of KLP10A and Patronin molecules that diffuse freely in the one-dimensional space and bind and dissociate from the MTs at rates k_{on} and k_{off}. The MTs in the model are assumed to slide polewards and polymerize at their plus ends at the sliding rate, effectively giving rise to a fixed position of the MT plus end in the laboratory frame of reference (Fig. S3 C). MT minus ends depolymerize at a rate determined by the number of "active" KLP10A molecules bound. The aim is to test (a) whether depolymerization of the sliding MTs' minus ends at a rate determined by the bound and active KLP10A to Patronin ratio can yield a stable "front" of MT minus ends, despite stochastic effects, and (b) whether changes in the activity of Patronin relative to KLP10A can tip this balance, resulting in the outward movement of the MT minus-end front at the experimentally observed rate during anaphase B. As in all mathematical models, several simplifying/modeling assumptions were made.

Simplifying assumptions. (a) The spindle is assumed to be fully symmetric with respect to the spindle equator; hence, we only consider MT length and position changes in a half-spindle. (b) The model is effectively one

dimensional, accounting for changes in MT length and position along the spindle pole–pole axis, and all MTs are assumed to lie parallel to this axis. (c) MT plus-end dynamic instability is not accounted for explicitly, and the model only considers the resulting net growth rate of MT plus ends to maintain an antiparallel overlap for steady poleward sliding of MTs. (d) All MTs are assumed to slide polewards at the observed mean sliding rate by the action of sliding motors on antiparallel overlaps and cross-linkers to parallel adjacent MTs. (e) Changes in the activity of Patronin and KLP10A molecules are assumed to occur at much faster time scales than MT depolymerization and sliding and are not accounted for explicitly.

Other assumptions. (f) The total number of KLP10A and Patronin molecules available in the spindle volume is assumed to be constant during metaphase–anaphase B. (g) Free KLP10A and Patronin molecules are assumed to be well mixed by diffusion along the axis perpendicular to the pole–pole axis, and only diffusion along the pole–pole axis is explicitly considered. (The ratio between the spindle pole–pole axis and the perpendicular axis is ∼2 during metaphase and increases to >3 during anaphase; thus, the diffusion along the pole–pole axis limits the binding reactions more strongly.) (h) The inhibitory activity of Patronin on the depolymerizing activity of KLP10A is depicted by the parameter γ and is assumed to increase spontaneously at the onset of anaphase B, in response to Cyclin B degradation. (i) The depolymerization (dissociation of tubulin subunits) from MT minus ends occurs at a rate proportional to the total number of active KLP10A molecules bound to a small region of length L_{cr} at the MT minus end. A baseline depolymerization rate is set by v^{δ}_{dep}, defining the depolymerization rate when δ number of active KLP10A is bound to the region of length L_{cr} at the MT minus end. Rates for different numbers of bound "active" KLP10A are scaled linearly with this baseline rate. Thus, in our model, tubulin dissociation by KLP10A is accounted for in a phenomenological approach, and individual tubulin dissociation events are not modeled. Therefore, in the interest of computation time, we consider an average approach and represent multiple dissociation events from the MT minus ends, proportional to the number of bound and active KLP10A in a small region at the minus end of the MT. The size of the critical length, L_{cr}, is chosen to limit the depolymerization rate to 10 × 8 nm = 80 nm—or ∼0.08 µm—per second, at full occupancy, whereas the experimentally observed depolymerization/poleward mean flux rate during metaphase, 0.06 µm/s, is lower than this value.

Modeling methods: Numerical simulations

The model simulation is set to mimic the MTs in the left metaphase half-spindle. A one-dimensional grid along the x axis is used to record the position and length changes of the MTs. MTs lie parallel to one another (Fig. S3 C), and there are typically 3–15 MTs tracked in each simulation. The one-dimensional spatial grid along the x axis is divided into M subcompartments of length Δx (typically, Δx = 6 nm). For each MT, an array of size M × T_{step} is generated to record the tubulin occupancy: if the i^{th} row, j^{th} column element is equal to 1, the MT occupies the subcompartment in question; if it is equal to 0, the MT does not extend to the subcompartment in question. Thus, the occupancy state of each subcompartment along the grid determines the current length and the position of the MT. The simulation is run for N_{step} iterations, with each iteration step corresponding to Δt seconds in real time (total time corresponds to (N_{step} × Δt) seconds.

Initial conditions. Initially, all MT plus and minus ends are located at x = 6 µm and x = 0 µm, respectively. No KLP10A or Patronin is bound to the MTs. All are in freely diffusible form.

Iteration algorithm. At each time step, as the MT slides poleward, polymerizes, and depolymerizes at the plus and minus ends, respectively, the MT occupancy state of each subcompartment along the grid for each MT is updated for the next time step according to their sliding, polymerization, and depolymerization rates.

MT sliding and plus-end polymerization. At each time step, the occupancy of the subcompartments of each MT is shifted left at the experimentally observed mean velocity of MT sliding (0.06 µm/s). Similarly, new subcompartment occupancy is added for each MT plus-end tip, i.e., the right end of the MT along the x axis, representing a net mean rate of MT plus-end polymerization. The number of subcompartment occupancy added at each time step is equivalent to the number of subcompartments that are shifted left by sliding, thereby mimicking a steady mean antiparallel MT overlap.

MT minus-end depolymerization. For each MT, the minus-end depolymerization rate is determined by the current number of active KLP10A molecules bound to the MT minus end within a critical region of length L_{cr}. At each time step, for each MT, the depolymerization rate is computed using

$$v_{dep}(t) = v^{\delta}_{dep}\frac{n_{10A}}{\delta},$$

in which v^{δ}_{dep} is the depolymerization rate when δ number of active KLP10A molecules are bound to the region of length L_{cr} at the MT tip, and n_{10A} is the current number of active KLP10A molecules bound to that region. The active number of KLP10A molecules, n_{10A}, is calculated as the difference between the total number of KLP10A and active inhibiting Patronin bound to the MT tip and is limited by 0 at the lower end. Once the current depolymerization rate and length is computed for each MT, the number of subcompartments, corresponding to the depolymerization length is computed, and the occupancy of the subcompartments at the minus end of the MT are set to 0.

KLP10A/Patronin diffusion and MT-binding/dissociation kinetics. The free KLP10A and Patronin molecules undergo diffusion along the x axis with diffusion constants D_K and D_P. A simple forward Euler algorithm is used to account for the one-dimensional diffusion of KLP10A and Patronin. The position of each KLP10A and Patronin molecule along the x axis is recorded at each time step (pos(K_k)(t) and pos(P_k)(t), for the kth KLP10A and Patronin molecule at time t), and for freely diffusing molecules, the position for the next time step is updated according to

$$\mathrm{pos}(K_k)(t+\Delta t) = \mathrm{pos}(K_k)(t) + \zeta\sqrt{2D_K\Delta t},$$

in which ζ is a normally distributed random number (function *randn* in MATLAB; Erban et al., 2007). Each "free" KLP10A and Patronin molecule can stochastically bind to a randomly selected MT, which occupies the subcompartment the molecule is currently in according to rate constants k^K_{on}, k^P_{on}, and k^K_{off} k^P_{off}. For each free molecule, first the position is compared with the occupancy of all the MTs in the corresponding subcompartment, and the candidate MTs are identified. A random MT is selected among these candidates using the *rand* function in MATLAB, and another uniform random number, r_1, selected using *rand*, is compared with the binding probability computed as $P_{on} = 1-\exp\left(k^K_{on}\right)\left(\text{or } P_{on} = 1-\exp\left(k^P_{on}\right)\right)$. If $r_1 < P_{on}$, the binding event is realized, the KLP10A (or Patronin) molecule is switched to a bound state, and the MT and the subcompartment it is bound to is recorded. Similarly, at each time step, for each bound KLP10A (and Patronin molecule) another uniform random number, r_2, is selected using *rand* and compared with the dissociation probability computed as $P_{off} = 1-\exp\left(k^K_{off}\right)\left(\text{or } P_{off} = 1-\exp\left(k^P_{off}\right)\right)$. If $r_2 < P_{off}$, the dissociation event is realized, the KLP10A (or Patronin) molecule is switched to a free state, and its position is recorded as the midpoint of the subcompartment it dissociated from. As MTs slide polewards, the new position of all MT-bound KLP10A and Patronin molecules are updated. As the MT minus end depolymerizes, the KLP10A and Patronin molecules bound to the depolymerizing subcompartment are switched to the free state. As the MT tip polymerizes and new subcompartments are added to the plus end of the MT, KLP10A and Patronin are not permitted to stochastically bind to the newly added subcompartments until the next time step.

Modeling methods: In silico FRAP of KLP10A and Patronin

After the main simulation is run and saved, an in silico FRAP of KLP10A (or Patronin) can be run. A bleach region (L_{bleach} R_{bleach}) is defined by the left and right boundaries along the x axis. A new array recoding the fluorescence state of all KLP10A (or Patronin) molecules is generated, and all fluorescence values are initially set to be equal to 1 (fluorescent). An algorithm running from the beginning to the final iteration time step then computes the fluorescence level within the bleach region as follows:

Before bleach time, T_{bleach} = n_{bleach} × Δt, the total number of all free and bound KLP10A (or Patronin) molecules whose positions are within the bleach region are labeled and recorded, and the sum of their fluorescence state represents the fluorescence level as a result of KLP10A (or Patronin) within the bleach region before the bleach. At the time of bleach, all free and bound KLP10A (or Patronin) molecules in the bleach region are labeled, and their fluorescent state is set to 0. At each subsequent time step, the KLP10A (or Patronin) molecules within the bleach region are labeled and recorded, and the sum of their fluorescence state represents the fluorescence level after photobleaching; as the bleached KLP10A (or Patronin) molecules fluorescence state was set to 0, they do not contribute to the sum.

Once the computation is completed for all time steps, the mean of the fluorescence level of KLP10A (or Patronin) in 5–10 time steps before the bleach is calculated, and the array in which KLP10A (or Patronin) fluorescence was logged is divided by this value to mimic the normalized fluorescence of KLP10A (or Patronin) within the bleach region. A plot of the resulting normalized fluorescence of KLP10A (or Patronin) over time represents the in silico FRAP, to be compared with the experimental FRAP data.

Online supplemental material

Fig. S1 shows the specificity of purified antibodies and effects of microinjections of the antibodies or purified cyclin B. Fig. S2 shows that KLP10A inhibition led to anaphase B spindle elongation in preanaphase B–arrested spindles (see also Video 7, in support of Fig. 4 B), independent of cortical forces and robust midzone assembly. Fig. S3 illustrates the details of the computational model to address the change in Patronin activity at anaphase B onset. Table S1 presents all parameters used in the computational modeling. Video 1 and Video 2 are related to Fig. 1 (A and B), respectively, showing the dynamics of KLP10A-GFP (Video 1) or Patronin-GFP (Video 2) in a representative spindle during *Drosophila* embryo mitosis. Video 3 and Video 4 are related to Fig. 2 A, comparing the spindle dynamics and chromosome segregation after Patronin inhibition (Video 4) with control (Video 3). Video 5 is related to Fig. 4 A (right), showing that KLP10A inhibition caused anaphase B–like elongation of metaphase-arrested spindles. Video 6 and Video 7 are related to Fig. 4 B (right) and Fig. S2 A, respectively, showing that KLP10A inhibition caused anaphase B–like elongation of anaphase A–arrested spindles. Online supplemental material is available at http://www.jcb.org/cgi/content/full/jcb.201306001/DC1. Additional data are available in the JCB DataViewer at http://dx.doi.org/10.1083/jcb.201306001.dv.

This work was supported by National Institutes of Health grant GM55507 to J.M. Scholey.

Submitted: 3 June 2013
Accepted: 10 September 2013

References

Acar, S., D.B. Carlson, M.S. Budamagunta, V. Yarov-Yarovoy, J.J. Correia, M.R. Niñonuevo, W. Jia, L. Tao, J.A. Leary, J.C. Voss, et al. 2013. The bipolar assembly domain of the mitotic motor kinesin-5. *Nat. Commun.* 4:1343. http://dx.doi.org/10.1038/ncomms2348

Brugués, J., V. Nuzzo, E. Mazur, and D.J. Needleman. 2012. Nucleation and transport organize microtubules in metaphase spindles. *Cell*. 149:554–564. http://dx.doi.org/10.1016/j.cell.2012.03.027

Brust-Mascher, I., and J.M. Scholey. 2002. Microtubule flux and sliding in mitotic spindles of *Drosophila* embryos. *Mol. Biol. Cell*. 13:3967–3975. http://dx.doi.org/10.1091/mbc.02-05-0069

Brust-Mascher, I., G. Civelekoglu-Scholey, M. Kwon, A. Mogilner, and J.M. Scholey. 2004. Model for anaphase B: role of three mitotic motors in a switch from poleward flux to spindle elongation. *Proc. Natl. Acad. Sci. USA*. 101:15938–15943. http://dx.doi.org/10.1073/pnas.0407044101

Brust-Mascher, I., P. Sommi, D.K. Cheerambathur, and J.M. Scholey. 2009. Kinesin-5-dependent poleward flux and spindle length control in *Drosophila* embryo mitosis. *Mol. Biol. Cell*. 20:1749–1762. http://dx.doi.org/10.1091/mbc.E08-10-1033

Burbank, K.S., T.J. Mitchison, and D.S. Fisher. 2007. Slide-and-cluster models for spindle assembly. *Curr. Biol.* 17:1373–1383. http://dx.doi.org/10.1016/j.cub.2007.07.058

Cheerambathur, D.K., G. Civelekoglu-Scholey, I. Brust-Mascher, P. Sommi, A. Mogilner, and J.M. Scholey. 2007. Quantitative analysis of an anaphase B switch: predicted role for a microtubule catastrophe gradient. *J. Cell Biol.* 177:995–1004. http://dx.doi.org/10.1083/jcb.200611113

Civelekoglu-Scholey, G., L. Tao, I. Brust-Mascher, R. Wollman, and J.M. Scholey. 2010. Prometaphase spindle maintenance by an antagonistic motor-dependent force balance made robust by a disassembling lamin-B envelope. *J. Cell Biol.* 188:49–68. http://dx.doi.org/10.1083/jcb.200908150

Cole, D.G., W.M. Saxton, K.B. Sheehan, and J.M. Scholey. 1994. A "slow" homotetrameric kinesin-related motor protein purified from *Drosophila* embryos. *J. Biol. Chem.* 269:22913–22916.

de Lartigue, J., I. Brust-Mascher, and J.M. Scholey. 2011. Anaphase B spindle dynamics in *Drosophila* S2 cells: Comparison with embryo spindles. *Cell Div.* 6:8. http://dx.doi.org/10.1186/1747-1028-6-8

Desai, A., S. Verma, T.J. Mitchison, and C.E. Walczak. 1999. Kin I kinesins are microtubule-destabilizing enzymes. *Cell*. 96:69–78. http://dx.doi.org/10.1016/S0092-8674(00)80960-5

Drechsler, H., and A.D. McAinsh. 2012. Exotic mitotic mechanisms. *Open Biol.* 2:120140. http://dx.doi.org/10.1098/rsob.120140

Dumont, S., and T.J. Mitchison. 2009. Compression regulates mitotic spindle length by a mechanochemical switch at the poles. *Curr. Biol.* 19:1086–1095. http://dx.doi.org/10.1016/j.cub.2009.05.056

Erban, R., J. Chapman, and P. Maini. 2007. A practical guide to stochastic simulations of reaction-diffusion processes. *arXiv Quantitative Biology: Subcellular Processes.* arXiv:0704.1908. Available at: http://arxiv.org/abs/0704.1908 (accessed September 13, 2013).

FitzHarris, G. 2012. Anaphase B precedes anaphase A in the mouse egg. *Curr. Biol.* 22:437–444. http://dx.doi.org/10.1016/j.cub.2012.01.041

Gadde, S., and R. Heald. 2004. Mechanisms and molecules of the mitotic spindle. *Curr. Biol.* 14:R797–R805. http://dx.doi.org/10.1016/j.cub.2004.09.021

Goodwin, S.S., and R.D. Vale. 2010. Patronin regulates the microtubule network by protecting microtubule minus ends. *Cell*. 143:263–274. http://dx.doi.org/10.1016/j.cell.2010.09.022

Goshima, G., and J.M. Scholey. 2010. Control of mitotic spindle length. *Annu. Rev. Cell Dev. Biol.* 26:21–57. http://dx.doi.org/10.1146/annurev-cellbio-100109-104006

Goshima, G., and R.D. Vale. 2005. Cell cycle-dependent dynamics and regulation of mitotic kinesins in *Drosophila* S2 cells. *Mol. Biol. Cell*. 16:3896–3907. http://dx.doi.org/10.1091/mbc.E05-02-0118

Goshima, G., R. Wollman, S.S. Goodwin, N. Zhang, J.M. Scholey, R.D. Vale, and N. Stuurman. 2007. Genes required for mitotic spindle assembly in *Drosophila* S2 cells. *Science*. 316:417–421. http://dx.doi.org/10.1126/science.1141314

Hartigan, P.M. 1985. Algorithm AS 217: Computation of the dip statistic to test for unimodality. *J. R. Stat. Soc. Ser. C Appl. Stat.* 34:320–325.

Hartigan, J.A., and P.M. Hartigan. 1985. The dip test of unimodality. *Ann. Statist.* 13:70–84. http://dx.doi.org/10.1214/aos/1176346577

Henikoff, S., K. Ahmad, J.S. Platero, and B. van Steensel. 2000. Heterochromatic deposition of centromeric histone H3-like proteins. *Proc. Natl. Acad. Sci. USA*. 97:716–721. http://dx.doi.org/10.1073/pnas.97.2.716

Kashina, A.S., R.J. Baskin, D.G. Cole, K.P. Wedaman, W.M. Saxton, and J.M. Scholey. 1996. A bipolar kinesin. *Nature*. 379:270–272. http://dx.doi.org/10.1038/379270a0

Kellogg, D.R., A. Kikuchi, T. Fujii-Nakata, C.W. Turck, and A.W. Murray. 1995. Members of the NAP/SET family of proteins interact specifically with B-type cyclins. *J. Cell Biol.* 130:661–673. http://dx.doi.org/10.1083/jcb.130.3.661

Lele, T., S.R. Wagner, J.A. Nickerson, and D.E. Ingber. 2006. Methods for measuring rates of protein binding to insoluble scaffolds in living cells: histone H1-chromatin interactions. *J. Cell. Biochem.* 99:1334–1342. http://dx.doi.org/10.1002/jcb.20997

Loughlin, R., R. Heald, and F. Nédélec. 2010. A computational model predicts *Xenopus* meiotic spindle organization. *J. Cell Biol.* 191:1239–1249. http://dx.doi.org/10.1083/jcb.201006076

Loughlin, R., J.D. Wilbur, F.J. McNally, F.J. Nédélec, and R. Heald. 2011. Katanin contributes to interspecies spindle length scaling in *Xenopus*. *Cell*. 147:1397–1407. http://dx.doi.org/10.1016/j.cell.2011.11.014

Mallavarapu, A., K. Sawin, and T. Mitchison. 1999. A switch in microtubule dynamics at the onset of anaphase B in the mitotic spindle of *Schizosaccharomyces pombe*. *Curr. Biol.* 9:1423–1426. http://dx.doi.org/10.1016/S0960-9822(00)80090-1

McIntosh, J.R., M.I. Molodtsov, and F.I. Ataullakhanov. 2012. Biophysics of mitosis. *Q. Rev. Biophys.* 45:147–207. http://dx.doi.org/10.1017/S0033583512000017

Parry, D.H., and P.H. O'Farrell. 2001. The schedule of destruction of three mitotic cyclins can dictate the timing of events during exit from mitosis. *Curr. Biol.* 11:671–683. http://dx.doi.org/10.1016/S0960-9822(01)00204-4

Phair, R.D., and T. Misteli. 2000. High mobility of proteins in the mammalian cell nucleus. *Nature*. 404:604–609. http://dx.doi.org/10.1038/35007077

Ris, H. 1943. A quantitative study of anaphase movement in the aphid tamalia. *Biol. Bull.* 85:164–178. http://dx.doi.org/10.2307/1538278

Rogers, G.C., S.L. Rogers, T.A. Schwimmer, S.C. Ems-McClung, C.E. Walczak, R.D. Vale, J.M. Scholey, and D.J. Sharp. 2004. Two mitotic kinesins cooperate to drive sister chromatid separation during anaphase. *Nature*. 427:364–370. http://dx.doi.org/10.1038/nature02256

Rogers, S.L., G.C. Rogers, D.J. Sharp, and R.D. Vale. 2002. *Drosophila* EB1 is important for proper assembly, dynamics, and positioning of the mitotic spindle. *J. Cell Biol.* 158:873–884. http://dx.doi.org/10.1083/jcb.200202032

Saunders, A.M., J. Powers, S. Strome, and W.M. Saxton. 2007. Kinesin-5 acts as a brake in anaphase spindle elongation. *Curr. Biol.* 17:R453–R454. http://dx.doi.org/10.1016/j.cub.2007.05.001

Sharp, D.J., H.M. Brown, M. Kwon, G.C. Rogers, G. Holland, and J.M. Scholey. 2000. Functional coordination of three mitotic motors in *Drosophila* embryos. *Mol. Biol. Cell*. 11:241–253. http://dx.doi.org/10.1091/mbc.11.1.241

Stevenson, V.A., J. Kramer, J. Kuhn, and W.E. Theurkauf. 2001. Centrosomes and the Scrambled protein coordinate microtubule-independent actin reorganization. *Nat. Cell Biol.* 3:68–75. http://dx.doi.org/10.1038/35050579

Tao, L., A. Mogilner, G. Civelekoglu-Scholey, R. Wollman, J. Evans, H. Stahlberg, and J.M. Scholey. 2006. A homotetrameric kinesin-5, KLP61F, bundles microtubules and antagonizes Ncd in motility assays. *Curr. Biol.* 16:2293–2302. http://dx.doi.org/10.1016/j.cub.2006.09.064

Telley, I.A., I. Gáspár, A. Ephrussi, and T. Surrey. 2012. Aster migration determines the length scale of nuclear separation in the *Drosophila* syncytial embryo. *J. Cell Biol.* 197:887–895. http://dx.doi.org/10.1083/jcb.201204019

van den Wildenberg, S.M., L. Tao, L.C. Kapitein, C.F. Schmidt, J.M. Scholey, and E.J. Peterman. 2008. The homotetrameric kinesin-5 KLP61F preferentially crosslinks microtubules into antiparallel orientations. *Curr. Biol.* 18:1860–1864. http://dx.doi.org/10.1016/j.cub.2008.10.026

Varga, V., J. Helenius, K. Tanaka, A.A. Hyman, T.U. Tanaka, and J. Howard. 2006. Yeast kinesin-8 depolymerizes microtubules in a length-dependent manner. *Nat. Cell Biol.* 8:957–962. http://dx.doi.org/10.1038/ncb1462

Vernì, F., M.P. Somma, K.C. Gunsalus, S. Bonaccorsi, G. Belloni, M.L. Goldberg, and M. Gatti. 2004. Feo, the *Drosophila* homolog of PRC1, is required for central-spindle formation and cytokinesis. *Curr. Biol.* 14:1569–1575. http://dx.doi.org/10.1016/j.cub.2004.08.054

Walczak, C.E., S. Cai, and A. Khodjakov. 2010. Mechanisms of chromosome behaviour during mitosis. *Nat. Rev. Mol. Cell Biol.* 11:91–102. http://dx.doi.org/10.1038/nrm2832

Wang, H., I. Brust-Mascher, D. Cheerambathur, and J.M. Scholey. 2010. Coupling between microtubule sliding, plus-end growth and spindle length revealed by kinesin-8 depletion. *Cytoskeleton (Hoboken)*. 67:715–728. http://dx.doi.org/10.1002/cm.20482